Lawrence Berkeley National Laboratory

Title
Carbon Thaw Rate Doubles When Accounting for Subsidence in a Permafrost Warming Experiment

Permalink
https://escholarship.org/uc/item/0mp6r6qh

Journal
Journal of Geophysical Research Biogeosciences, 125(6)

ISSN
2169-8953

Authors
Rodenhizer, Heidi
Ledman, Justin
Mauritz, Marguerite
et al.

Publication Date
2020-06-01

DOI
10.1029/2019jg005528

Peer reviewed

JGR Biogeosciences

Key Points:
- Subsidence causes a shifting reference frame for measurements of permafrost thaw
- The rate of permafrost carbon thaw doubles when subsidence is accounted for
- Subsidence of up to 6 cm year^{-1} was observed in a permafrost warming experiment, due to both ice and soil loss

Correspondence to:
H. Rodenhizer,
hgr7@nau.edu

Carbon Thaw Rate Doubles When Accounting for Subsidence in a Permafrost Warming Experiment

Heidi Rodenhizer[1] [ID], Justin Ledman[1,2], Marguerite Mauritz[1,3] [ID], Susan M. Natali[4] [ID], Elaine Pegoraro[1], César Plaza[5] [ID], Emily Romano[1], Christina Schädel[1,6] [ID], Meghan Taylor[1,7] [ID], and Edward Schuur[1]

[1]Center for Ecosystem Science and Society, Northern Arizona University, Flagstaff, AZ, USA, [2]Bonanza Creek Long Term Ecological Research Site, University of Alaska Fairbanks, Fairbanks, AK, USA, [3]Now at Biology Department, University of Texas at El Paso, El Paso, TX, USA, [4]Woods Hole Research Center, Falmouth, MA, USA, [5]Instituto de Ciencias Agrarias, Consejo Superior de Investigaciones Científicas, Madrid, Spain, [6]School of Informatics, Computing, and Cyber Systems, Northern Arizona University, Flagstaff, AZ, USA, [7]Now at School of Forestry and Environmental Studies, Yale University, New Haven, CT, USA

Abstract Permafrost thaw is typically measured with active layer thickness, or the maximum seasonal thaw measured from the ground surface. However, previous work has shown that this measurement alone fails to account for ground subsidence and therefore underestimates permafrost thaw. To determine the impact of subsidence on observed permafrost thaw and thawed soil carbon stocks, we quantified subsidence using high-accuracy GPS and identified its environmental drivers in a permafrost warming experiment near the southern limit of permafrost in Alaska. With permafrost temperatures near 0°C, 10.8 cm of subsidence was observed in control plots over 9 years. Experimental air and soil warming increased subsidence by five times and created inundated microsites. Across treatments, ice and soil loss drove 85–91% and 9–15% of subsidence, respectively. Accounting for subsidence, permafrost thawed between 19% (control) and 49% (warming) deeper than active layer thickness indicated, and the amount of newly thawed carbon within the active layer was between 37% (control) and 113% (warming) greater. As additional carbon thaws as the active layer deepens, carbon fluxes to the atmosphere and lateral transport of carbon in groundwater could increase. The magnitude of this impact is uncertain at the landscape scale, though, due to limited subsidence measurements. Therefore, to determine the full extent of permafrost thaw across the circumpolar region and its feedback on the carbon cycle, it is necessary to quantify subsidence more broadly across the circumpolar region.

Plain Language Summary Permafrost soils, which are perennially frozen soils found throughout cold regions, contain vast quantities of carbon and ice. When permafrost thaws, carbon can be lost to the atmosphere, contributing to climate change. This means it is important to track permafrost thaw, which is often done using active layer thickness, or the depth of the seasonally thawed surface layer of soil. However, ice volume can be lost from thawing permafrost, causing the soil surface to drop. Conventional measurements do not account for this surface drop, and the rate of thaw could therefore be underestimated. We found that experimentally warmed soils dropped at a rate of 6 cm year^{-1}, mostly due to loss of ice volume and also due to the loss of soil mass. When accounting for the change in soil surface height over time, the full depth of permafrost thaw was 49% greater. The increased depth of thaw resulted in more than twice as much carbon being thawed as was estimated with standard methods that did not account for subsidence. These findings suggest that permafrost is thawing more quickly than long-term records indicate and that this could result in additional carbon release contributing to climate change.

1. Introduction

Arctic temperatures are rising about 2.5 times faster than the global average (Intergovernmental Panel on Climate Change, 2013), and experimental evidence shows that this is causing permafrost ecosystems to shift from an atmospheric carbon (C) sink to a C source (Belshe et al., 2013; Commane et al., 2017; Euskirchen et al., 2017; Schuur & Mack, 2018). Much of the Arctic is underlain by permafrost soils, where freezing conditions have maintained a slow but consistent C sink by protecting soil C from microbial respiration for up to

thousands of years (Hicks Pries et al., 2012; Schuur et al., 2015; Tarnocai et al., 2009; Zimov et al., 2006). Permafrost soils contain 1,440–1,600 Pg C globally (Schuur et al., 2018), which is about twice as much C as is in the atmosphere (Houghton, 2007). However, rapidly increasing temperatures in the Arctic have begun to thaw permafrost and alter ecosystem C balance, determined from the relative contributions of plant production and ecosystem respiration. While plant productivity is expected to increase under future climate change, changes in microbial respiration are likely to be an order of magnitude higher, causing permafrost ecosystems to shift to a C source over the next century (Belshe et al., 2013; Schuur et al., 2018).

Active layer thickness (ALT), the depth of seasonal permafrost thaw, has been closely monitored as one of the key variables for understanding the impact of climate change on permafrost thaw and ecosystem C dynamics (Brown et al., 2000; Nixon & Taylor, 1998). ALT plays an important role in regulating the response of plant production and respiration to climate change in the Arctic. As the region warms, ALT tends to increase (Brown et al., 2000; Romanovsky et al., 2003; Shiklomanov et al., 2012; Streletskiy et al., 2008), thawing both C and nutrients (Salmon et al., 2018). Greater access to nitrogen can increase plant growth (Chapin et al., 1995; Shaver et al., 1992), while increasing C availability to microbes increases respiration of C that had been thermally protected from decomposition (Hicks Pries et al., 2013; Hicks Pries et al., 2016). Therefore, the Circumpolar Active Layer Monitoring (CALM) network was established to track changes in ALT and near surface permafrost at over 200 sites (Brown et al., 2000).

Permafrost thaw also induces physical changes to the soil profile, impacting its structural stability by causing the ground to compact and subside (Kokelj & Jorgenson, 2013). It is widely accepted that subsidence occurs as permafrost soils thaw, and ice volume is lost (Jorgenson & Osterkamp, 2005; Kokelj & Jorgenson, 2013; Nelson et al., 2001), because permafrost soils contain up to 80% ice by volume (Schuur et al., 2008). Depending on the distribution of ice across the landscape, and other environmental factors including local topography, the morphology of subsidence can vary considerably (Jorgenson & Osterkamp, 2005; Kokelj & Jorgenson, 2013). Many types of thermokarst occurring in soils with high and variable ice content result in highly visible disturbances, including thaw slumps and thermokarst lakes, pits, and gullies (Jones et al., 2012; Jorgenson & Osterkamp, 2005; Ward Jones et al., 2019). These thermokarst features occur in areas estimated to cover ~20% of the circumpolar region (Olefeldt et al., 2016). However, in soils with relatively low to medium ice content, particularly rocky or gravelly areas, thaw can lead to more gradual, nonpatterned subsidence (Jorgenson & Osterkamp, 2005), which has also been termed isotropic subsidence (Shiklomanov et al., 2013; Streletskiy et al., 2017). Nonpatterned subsidence, due to the lack of visually obvious features, is more challenging to detect without monitoring elevation changes (Jorgenson & Osterkamp, 2005; Shiklomanov et al., 2013). It is also conceivable that areas of recent or gradual permafrost thaw could appear to be nonpatterned to observers on the ground, as subsidence may not have progressed sufficiently to be visible. The combined extent of gradual and nonpatterned subsidence is unknown because elevation change is not monitored extensively in permafrost regions, but due to recent, rapidly changing temperatures in the Arctic, it is potentially broad.

Soil loss could also contribute to subsidence through the release of C to the atmosphere and lateral transport of C in water, if losses are high enough to significantly decrease the volume of organic matter within the soil profile. A significant contribution of peat loss to subsidence has been shown previously in a drained ombrotrophic bog (Grønlund et al., 2008), but to the best of our knowledge, no studies have previously attempted to quantify the impact of soil loss on subsidence in permafrost ecosystems, so it is uncertain whether currently observed rates of soil loss are sufficient to decrease soil volume at a detectable level. However, both release of C to the atmosphere and export in water tend to be higher in areas of thermokarst than in adjacent, undisturbed areas (Abbott et al., 2015; Abbott & Jones, 2015; Cassidy et al., 2016; Euskirchen et al., 2017), meaning that these areas should be the first to show the effect of soil loss on subsidence.

Subsidence is rarely quantified when monitoring permafrost thaw, and this is problematic because long-term measurements of ALT have been shown to underestimate the rate of permafrost thaw (O'Neill et al., 2019; Shiklomanov et al., 2013; Streletskiy et al., 2017). The typical method of monitoring ALT is to insert a metal probe into the ground until it hits permafrost and measure the distance from the soil surface to the bottom of the probe (Hinkel & Nelson, 2003). However, long-term monitoring in some areas has shown little to no change in ALT despite increases in air and permafrost temperatures (O'Neill et al., 2019; Shiklomanov et al., 2013; Streletskiy et al., 2017). Subsidence can explain the lack of change in ALT, as it

causes a changing reference frame for ALT probe measurements through time, thereby masking the full depth of thaw (O'Neill et al., 2019; Shiklomanov et al., 2013; Streletskiy et al., 2017). Therefore, relying solely on ALT as a measure of permafrost thaw is also likely to underestimate the amount of soil C being mobilized in permafrost. To account for this discrepancy, some studies have used thaw tubes to measure thaw penetration, the sum of subsidence and ALT (Nixon & Taylor, 1998); however, most studies still rely on ALT without accounting for subsidence.

Subsidence drastically alters the hydrologic conditions within the active layer (Hinkel & Hurd, 2006; Johansson et al., 2013; O'Neill & Burn, 2017) and thereby regulates the fate of permafrost C upon thaw. In Earth System Models, permafrost thaw results in drier soils as the permafrost table drops and drainage is increased (Schädel et al., 2018); however, experimental data show that subsidence often results in wetter soils and the formation of ponds or lakes, at least in the short term (Hinkel & Hurd, 2006; Johansson et al., 2013; Jorgenson et al., 2013; Mauritz et al., 2017). Wetter conditions increase soil temperatures and accelerate thaw through the high latent heat of water (Subin et al., 2013), and anaerobic conditions in saturated soils cause more C to be released as methane (CH_4) rather than carbon dioxide (CO_2) (Blanc-Betes et al., 2016; Johnston et al., 2014; Kutzbach et al., 2004; Taylor et al., 2018). Although anaerobic conditions simultaneously slow the rate of decomposition, the increased production of CH_4, which is 45 times more powerful a greenhouse gas than CO_2 over a 100 year timescale (Myhre et al., 2013), more than outweighs the lower rates of C release (Schuur et al., 2008; Taylor et al., 2018). Therefore, both the magnitude and form of C release depend upon how hydrologic conditions develop as permafrost thaws and the ground subsides.

Here, we quantified subsidence and thaw penetration over 9 years at a permafrost warming experiment near Healy, AK. This site is located within the discontinuous permafrost zone where permafrost temperatures are near 0°C, providing ideal conditions to investigate the impact of experimental warming on subsidence, permafrost thaw, and C dynamics. The overall goal of this study was to determine the factors that drive subsidence and the impact of subsidence on permafrost thaw and the permafrost C feedback to climate. We specifically aimed to determine (1) the amount of subsidence which occurred over 9 years of permafrost warming and the impact of air and soil warming on this process, (2) the relative contributions of ice loss and soil loss to subsidence, and (3) the impact of using thaw penetration, rather than ALT, on estimates of C exposure in the deepening active layer. We hypothesized that (1) soil warming would accelerate subsidence over control conditions, but that air warming would not alter soil temperature sufficiently to impact the rate of subsidence, (2) ice loss would be responsible for nearly all of the observed subsidence and the impact of soil loss on subsidence would be too small to detect, even in areas of thermokarst, and (3) using thaw penetration rather than ALT would increase the estimate of recently thawed C in the active layer by a large margin, because previously observed rates of both subsidence in degrading permafrost and ALT expansion into the permafrost are on the order of centimeters per year.

2. Study Site

The Carbon in Permafrost Experimental Heating Research (CiPEHR) site is located near Healy, Alaska, USA, just outside Denali National Park (WGS84, 63°52′59″N, 149°13′32″W). The site is underlain by permafrost owing to the elevation of the foothills of the Alaska Range (670 m, Geoid 12B). The mean annual temperature is −0.94°C with a nonsummer (October–April) average temperature of −10.09°C and a summer (May–September) average temperature of 11.91°C (Healy and McKinley Stations, Western Regional Climate Center and NOAA National Centers for Environmental Information) (Mauritz et al., 2017). The ecosystem is classified as moist acidic tussock tundra, with the predominant vegetation types being the tussock forming *Eriophorum vaginatum* and the deciduous shrub, *Vaccinium uliginosum* (Salmon et al., 2016; Schuur et al., 2007). Soils are Gelisols, with an organic layer of approximately 0.35 m above cryoturbated mineral soils that are composed of glacial till and windblown loess (Natali et al., 2011; Plaza et al., 2017).

CiPEHR was established in 2008 to study ecosystem C responses to rising Arctic temperatures by experimentally warming both soil and air temperatures (Natali et al., 2011). Six snow fences 1.5 m tall and 8 m long were set up every winter in three replicate blocks (A, B, and C) that contain two fences, each 5 m apart (Figure 1). The snow fences trap snow on the leeward side, insulating the ground from very cold winter temperatures. Snow depth on the soil warming side typically reached the height of the snow fences by midwinter, regardless of the ambient snow depth in any particular year (Figure 2). Snow was removed each April to
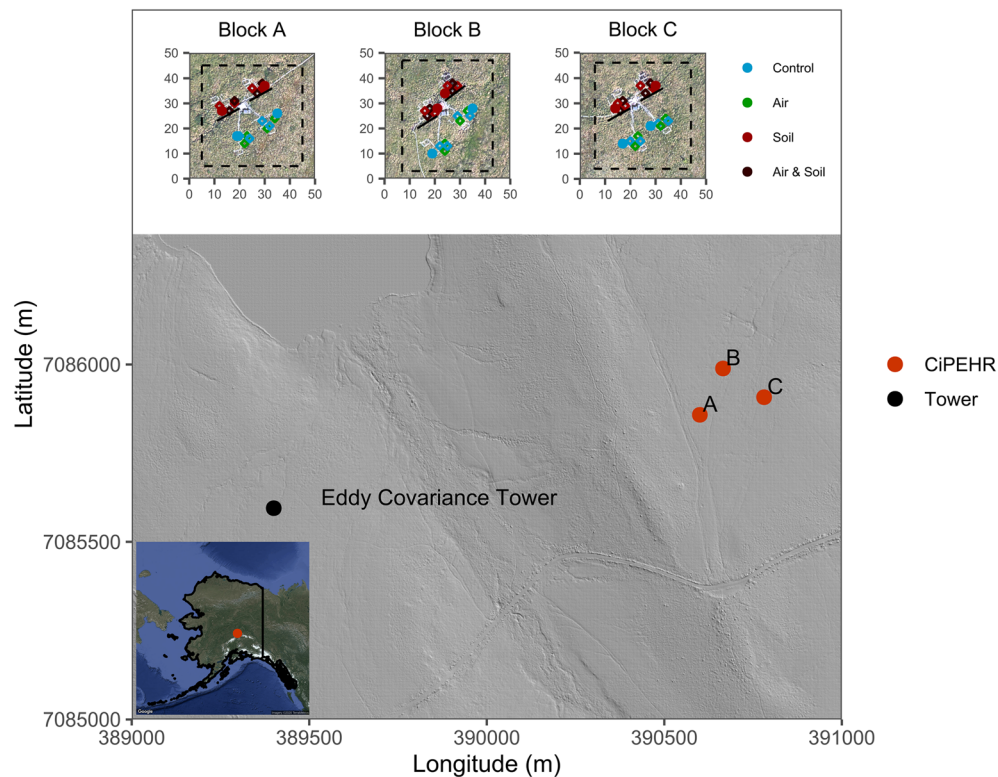
Figure 1. The location of the three blocks of CiPEHR and the eddy covariance tower located ~1 km away with the topography shown using a hillshade derived from National Ecological Observatory Network (NEON) airborne Light Detection and Ranging (LiDAR) (NEON, 2017a). The site is just west of Healy, AK, and Eight Mile Lake is visible at the top left. Axis labels indicate location (m) in UTM zone 6N. The three insets at the top show the location of soil cores (dots) and plots (open diamonds) within each block over high-resolution aerial photographs available from NEON (2018). The solid black lines show the location of snow fences, and the dashed lines indicate the maximum extent of the GPS transects. The inset at bottom left shows the location within Alaska.

avoid additional water input and delayed snow melt. At each snow fence, four 0.36 m^2 plots were located on the soil warming side and four plots were located on the control side. Additionally, two of the four plots on either side of the fence received air warming using 0.5-m-tall clear polycarbonate open top chambers, which were placed over the plots throughout each summer season. After the first 2 years, deep soil (20 and 40 cm) temperatures remained an average of 0.78°C warmer in soil warming plots throughout the summer season (Mauritz et al., 2017; Natali et al., 2011). By 2015, after 7 years of treatment, soil warming had resulted in a nonsummer season increase of 1.49°C in surface soil temperatures (5 and 10 cm) and 1.05°C in deep soil temperatures (20 and 40 cm) (Mauritz et al., 2017). On average, air warming increased air temperatures by 0.3°C during the first summer season and likely does not cause significant soil warming (Natali et al., 2011).

3. Materials and Methods

3.1. Elevation Measurements and Subsidence Calculation

Subsidence was estimated as the change in elevation derived from high-accuracy GPS measurements (Rodenhizer et al., 2019a). We measured elevation at each experimental block at 2 m intervals in an approximately 30 × 30 m grid in 2009, 2011, and each of 2015–2018 using a Trimble high-resolution differential global position system (dGPS) with real-time kinematic correction. A base station was placed at a U.S. Geological Survey geodetic marker (WGS84, 63.88793°N, 149.2383°W) <1 km from CiPEHR in order to

Figure 2. Snowpack on the leeward side of the snow fences in April 2016, just prior to snow removal. Photo credit: M. Mauritz.

continuously correct for atmospheric disturbances. Each elevation grid point was measured for 3–5 s on top of the moss layer. In 2009 and 2011, postprocessing was completed with a methodology developed by UNAVCO using Trimble Geomatics Office (Dayton, Ohio). Beginning in 2015, postprocessing was completed using a more highly automated methodology developed by the National Park Service using Trimble Business Center (Sunnyvale, California). Trimble Business Center replaced Trimble Geomatics Office when it was discontinued, necessitating a new processing protocol, and, despite the shift to a new software platform and a more highly automated protocol, the underlying processing methodology was the same. We transformed all GPS data to the Alaska Zone 4 State Plane coordinate system with the GRS80 ellipsoid and geoid 12B. We interpolated elevation surfaces using the gstat package (Gräler et al., 2016; Pebesma, 2004) in R (R Core Team, 2018) by building exponential models of empirical semivariograms and interpolating between the points using anisotropic kriging in two directions (across slope and downslope) (Bivand et al., 2008). Standard error of kriging was calculated for each cell and is reported with subsidence values (supporting information Figure S1). Subsidence was calculated from the elevation surfaces relative to 2009 using the raster package (Hijmans, 2019). Subsidence for years missing GPS points was interpolated linearly cell by cell.

GPS accuracy of individual points was very high, although inconsistencies in data collection may have impacted the accuracy of subsidence. GPS accuracy was measured with two checkpoints located within a few meters of the base station and measured for 2 min continuously. GPS horizontal accuracy averaged 0.010 m and vertical accuracy averaged 0.0016 m; however, GPS points were not measured in consistent locations throughout the years of sampling. Through 2016, the grid points were set up by hand using a measuring tape, meaning that points were measured in slightly different locations from year to year. The roughness of the tundra vegetation surface means that elevation can differ by tens of centimeters at points that are only slightly offset from one another, and this could contribute variability to the final subsidence product. For example, sample semivariograms of the raw elevation data indicate that points separated by ~1 m differ by 5–7 cm on average, with certain pairs of points differing by nearly 1 m. In 2017, we realized the potential impact of this data collection method, and from 2017 on, the grid points were loaded onto the GPS ahead of time to allow quick navigation to the same point year after year. It is impossible to estimate the error associated with gap filling elevation in years without GPS data, as the cell-by-cell interpolation does not build linear models with all of the available data points but rather fills in missing values by drawing a line through the two closest (temporally) nonmissing data points. However, we expect that the error introduced by this step is insignificant relative to the error introduced by the varying offset of GPS points from 1 year to another.

3.2. ALT and Water Table Depth

Changes in permafrost thaw and hydrologic conditions were characterized with ALT and water table depth measurements between 2009 and 2018. Thaw depth was measured at each of the plots by inserting a metal probe into the ground until it hit frozen soil, and ALT was quantified as the thaw depth in mid-September (Week 36 of the year) at maximum depth of thaw (Mauritz et al., 2017; Natali & Schuur, 2012; Pegoraro, Mauritz, Hutchings, et al., 2019). Water table depth, the depth to ground water, was measured within PVC lined wells three times a week during the summer season (Schädel et al., 2018b). Between 2009 and 2012, water table depth was measured within two water wells on each side of the snow fences, and between 2013 and 2018, within three water wells on each side of the snow fences.

3.3. Soil Cores

We collected soil cores in May 2009 to measure ice and C content prior to experimentally induced permafrost thaw (Plaza et al., 2017). Two cores were taken per fence, one on the soil warming side and one on the control side. The thawed surface layer (~15 cm) was collected using a serrated knife, and the frozen ground underneath was cored using a Tanaka drill with a 7.6-cm-diameter hollow bit until gravel halted progress (~85 cm). Cores were stored frozen until processing in the laboratory. The surface vegetation was clipped to the bottom of the green moss, and cores were sectioned in a 5 cm increment at the surface and 10 cm increments thereafter. Each depth increment was subsampled for moisture content, bulk density, and C content (Hicks Pries et al., 2012; Pegoraro, Mauritz & Bracho, 2019). Soil gravimetric water content was measured as the water mass over the wet soil mass (g H_2O g wet soil^{-1}), because using the wet soil mass in gravimetric water content determination performs better in ice-rich mineral soils (Phillips et al., 2015). Bulk density of dry soil was calculated as the mass of a soil sample of known volume (i.e., the total core volume for the

section of core, including ice and rocks, as derived from the core dimensions; g cm^{-3}) separated from the mass and volume of rocks. Carbon content was determined using an elemental combustion analyzer (used to combust the samples; ECS4010, Costech Analytical Technologies, Inc., Valencia, CA, USA) coupled with an isotope ratio mass spectrometer (used to measure the C content; Delta V advantage, Thermo Scientific Inc., Waltham, MA, USA).

3.4. Soil Core Calculations

We combined GPS measurements with data on ice and C content from the soil cores to determine the role subsidence has in the quantification of permafrost thaw, as well as the potential driving factors of subsidence. Using the tidyverse package (Wickham, 2017) within R (R Core Team, 2018), we accounted for the effect that the shift in soil surface height had on ALT measurements, calculated the total amount of bulk soil C thawed over the study period, and partitioned total subsidence into the contributions from loss of ice and loss of soil.

To determine the full depth of permafrost thaw over the course of the experiment, we calculated thaw penetration as follows:

$$\text{Thaw Penetration} = \text{ALT} + \text{Subsidence}, \tag{1}$$

where ALT is the depth of thaw during Week 36 of the year (late August or early September) and subsidence is the cumulative interannual subsidence through the date of ALT probing (2009–20xx). To determine the cumulative interannual subsidence for each plot in each year, we extracted the value of subsidence in each year from the kriged surface at the location of each plot (Rodenhizer et al., 2019b). We calculated the amount of bulk soil C that thawed between 2009 (initial) and each following year (final) as the sum of C content at depths between the initial and final thaw penetration (Figure S2). Carbon content from 2009 was used so that the initial quantity of C in the permafrost was accounted for, even though some of the C that thawed between 2009 and the end of the experiment were lost following thaw, either to the atmosphere or laterally in water. This calculation was repeated using ALT, and the difference between the two calculations was taken in order to determine the impact of accounting for subsidence on the magnitude of C exposure upon permafrost thaw.

Potential subsidence due to ice loss was determined by calculating the volume of ice divided by the soil core area (ice height) from the soil cores taken in 2009 (representing initial conditions prior to warming). This calculation was based on the volume of ice contained in thawed permafrost, which was considered to be the layer of soil between the initial (2009) thaw penetration and the final (2013 or 2018) thaw penetration (Figure S2). We used final values of both 2013 and 2018, because many of the soil cores were only deep enough to reach the depth of 2013 thaw penetration. We calculated the volume of ice that can contribute to subsidence in two different ways to determine a maximum and minimum value of potential subsidence. The volume of ice for the maximum value was calculated using the total ice content and should be an overestimate of potential subsidence, because a significant portion of permafrost ice should exist within soil pores that will not collapse upon ice loss (Kokelj & Burn, 2003). The minimum value included only the estimated ice volume associated with excess ice (total ice-pore ice) and should theoretically be a closer estimate of potential subsidence.

To calculate the maximum potential subsidence due to ice loss, we had to first calculate the total mass of ice within the thawed permafrost. We started with the equation for gravimetric water content:

$$\text{GWC } (\%) = \frac{\text{Water Mass (g)}}{\text{Soil Mass (g)} + \text{Water Mass(g)}} \tag{2}$$

and replaced water mass with ice mass because, at the time of coring, all of the water content of the thawed permafrost layer was frozen in permafrost. We then rearranged Equation (2) to solve for ice mass:

$$\text{Ice Mass (g)} = \frac{\text{GWC } (\%) * \text{BD} \left(\frac{\text{g}}{\text{cm}^3}\right) * \text{Soil Core Volume (cm}^3)}{1 - \text{GWC } (\%)}, \tag{3}$$

where BD is the average bulk density of the thawed permafrost layer. Finally, the total ice height was calculated from the ice mass calculated in Equation (3):

$$\text{Total Ice Height (m)} = \frac{\text{Ice Mass (g)} * 0.92 \left(\frac{\text{cm}^3}{\text{g}}\right)}{100 \left(\frac{\text{cm}}{\text{m}}\right) * \text{Soil Core Area (cm}^2)}, \tag{4}$$

where 0.92 is the density of ice, and the whole equation is divided by 100 to convert from cm to m.

To remove the possibility of overestimating potential subsidence by including pore ice volume in the calculation, we partitioned the total ice height into components of pore ice and excess ice. As excess ice content was not measured following Kokelj and Burn (2003) when soil samples were originally taken, we instead estimated the excess ice by assuming the pore space of these soils is 50% of the soil volume (Text S1). This value was chosen because soils at a similar site ~1 km SE of CiPEHR are silt loam soils based on sand, silt, and clay percentages (National Ecological Observatory Network [NEON], 2017b), and silt loam soils are estimated to have 50% pore space (Brady & Weil, 2008). Any ice that did not fit into the estimated pore space was assumed to be excess ice and was included in the calculation of potential subsidence (Figure S3):

$$\text{Excess Ice Height (m)} = \frac{\text{Excess Ice (cm}^3)}{100 \left(\frac{\text{cm}}{\text{m}}\right) * \text{Soil Core Area (cm}^2)}, \tag{5}$$

where excess ice was calculated using Equations (S1)–(S4) and the soil core area was calculated from the diameter of the soil core.

To determine the contribution of soil loss to subsidence, we estimated the volume of organic soil from which measured C losses derived. Minimum and maximum C losses were estimated from previously published values derived from eddy covariance near CiPEHR (sum of CO_2 and CH_4 fluxes) or soil core measurements at CiPEHR, respectively (Plaza et al., 2019; Taylor et al., 2018). Eddy covariance towers are used to measure C fluxes at the landscape scale and, therefore, incorporate fluxes from varied microsites (Belshe et al., 2012). The eddy covariance tower is located ~1 km from CiPEHR and averages C fluxes in a footprint with a radius of approximately 200–350 m (Celis et al., 2017). Although the eddy covariance tower does not measure fluxes at CiPEHR, the vegetation composition, elevation, aspect, and C flux dynamics are very similar at both sites (Celis et al., 2017). At this site, CO_2 fluxes from eddy covariance are lower than those measured from soil cores, likely in part because eddy covariance measurements do not account for loss of C through lateral transport in ground water (Plaza et al., 2019). However, the C loss estimate from soil cores is about twice as large as that from eddy covariance, indicating a large lateral flux of C in water that has not been verified through other methods. Therefore, we used both estimates to constrain C flux estimates, with eddy covariance data as the lower bound and soil core data as the upper bound.

The potential height of soil previously occupied by lost C was calculated as follows:

$$\text{Soil Height (m)} = \frac{\text{C Loss} \left(\frac{\text{g}}{\text{m}^2 * \text{year}}\right)}{\text{C Content} \left(\frac{\text{g C}}{\text{g soil}}\right) * \text{BD} \left(\frac{\text{g}}{\text{m}^3}\right)} * 9 \text{ years}, \tag{6}$$

where C loss was the average rate of C loss from either eddy covariance or soil cores, C content was average soil C content in 2009, BD was the average bulk density in 2009, and 9 years was the length of the experiment. We divided by C content in order to account for the total mass of soil material that the C fluxes derived from and by the bulk density to estimate the height of soil within the core, which had been lost to C fluxes or lateral transport. Because this estimate uses the height of organic soil, not just C, and we have no direct measurements of the loss of elements other than C, both of these estimates could still be high. Average C content and bulk density were averaged from the soil cores at a depth of 5–35 cm, because this layer contains the highest organic matter content and we assume that mineral losses from soil are negligible (Plaza et al., 2019).

3.5. Statistical Analyses

We used mixed-effects models to analyze the effects of experimental warming on subsidence and permafrost thaw. All mixed-effects models were performed using the lme4 package (Bates et al., 2015), and we included a random effect for repeat measures and for the nested structure of the experiment (plot or soil core nested within fence nested within block). In each model, we examined the model residuals to test for normality and heteroscedasticity.

The impact of experimental air and soil warming on the rate of subsidence was investigated to determine the effect that future warming is likely to have on subsidence. Plot-level subsidence was used as the dependent variable, and the effects of time, treatment (control, air warming, soil warming, and air + soil warming), and the interaction between time and treatment were considered to evaluate whether rates of subsidence differed in each experimental treatment. Data for all plots were included in the model at each time step, yielding a total of 48 data points for each year that were evenly distributed across the four treatments. Model fit was evaluated with Akaike information criterion (AIC); parameter significance for the best model was shown with 95% confidence intervals (CIs) determined by bootstrapping with 1,000 simulations using the lme4 package (Bates et al., 2015). Differences in slope between groups were determined using the 95% CI in the emmeans package (Lenth, 2018).

The contribution of ice loss to subsidence was estimated using a mixed-effects model of subsidence by ice height. Separate models were tested using the total ice height and excess ice height. Subsidence was extracted from the kriged surface at each soil core location, and the effect of treatment was considered. This model had a total sample size of 24 soil cores, with half belonging to the control treatment and half to the soil warming treatment. AIC was used to determine the best fitting model, and model parameters were evaluated using 95% CIs determined by bootstrapping with 1,000 simulations using the lme4 package (Bates et al., 2015).

4. Results

4.1. Subsidence

Subsidence was observed across all blocks and treatments over 9 years of permafrost warming (Figure 3 and Movies S1–S3). Subsidence occurred at 1.2 cm year^{-1} (CI: 1.7, 0.7) in control plots and 1.4 cm year^{-1} (CI: 2.0, 0.9) in air warming plots, and the rate did not differ significantly between these two groups (Figure 4 and Table S1). Subsidence in soil warming plots occurred at 5.4 cm year^{-1} (CI: 5.9, 4.8), which was over 4 times the rate of the control plots and was significantly different than all other treatments. Air + soil warming plots had the greatest rate of subsidence at 6.1 cm year^{-1} (CI: 6.7, 5.6), which was ~5 times the rate of control plots and was also significantly different than all other treatments. The greatest subsidence observed across the footprints of the blocks was 89.2 ± 3.5 cm (mean ± SE of kriging) over 9 years (Figures 3 and 4). Starting in 2016, the formation of ponds on the soil warming side of Blocks B and C became evident. Elevation increases of up to 32.6 ± 5.1 cm were also observed within the first several years; however, this likely only reflects errors in the GPS time series, as most cells with elevation increases showed <10 cm of increase and the remaining cells occurred near the outer edge of the sampling locations where kriging variance is quite high in some years (Figures 3 and S1).

4.2. Permafrost and Carbon Thaw

Thaw penetration was significantly larger than ALT, the traditional method for measuring permafrost thaw (Figure 5). In control plots, ALT was 74.5 ± 1.2 cm and thaw penetration was 88.6 ± 2.3 cm, and in soil warming plots, ALT was 92.4 ± 2.7 cm and thaw penetration was 137.4 ± 4.3 cm by 2018 (Figure 5). Using thaw penetration to determine the depth of permafrost thaw over the course of the experiment increased observed thaw by 19 ± 3% in control plots and 49 ± 4% in warming plots. This could mean that rates of permafrost thaw are being underestimated across the circumpolar region, as subsidence is typically not quantified but can be expected wherever permafrost thaw is occurring.

Using thaw penetration to calculate C exposure in the active layer increased the amount of C thaw observed over the course of the study. We found an average of 50.2 ± 1.0 kg C m^{-2} in the active layer in control plots in 2009 (Figure 5). By 2018, there was 67.8 ± 0.9 kg C m^{-2} in the active layer as calculated with ALT and an average of 74.3 ± 1.1 kg C m^{-2} in the active layer as calculated with thaw penetration. Using ALT,
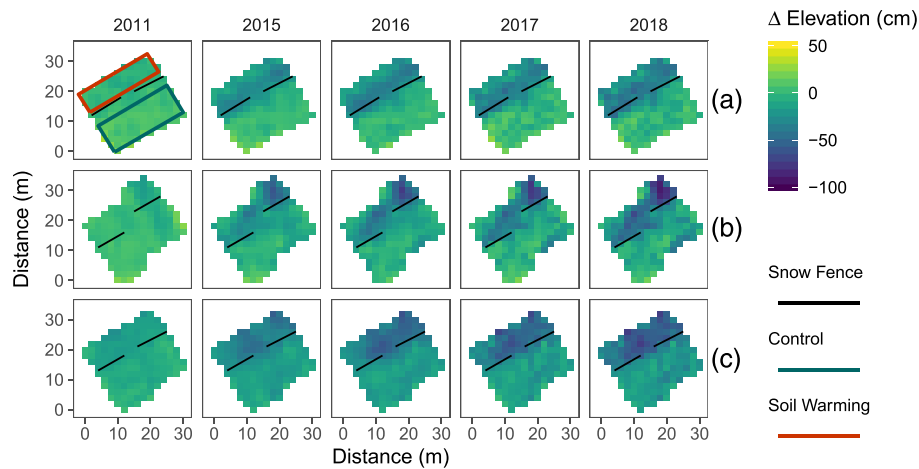
Figure 3. The change in elevation relative to 2009 at the three blocks (A, B, and C). Years with gap-filled data are not included. Negative values for elevation change indicate areas that have subsided. The locations of snow fences are indicated with solid black lines. The location of control plots and soil warming plots are indicated in the top left facet by blue and red rectangles, respectively, and these relative locations are the same for all blocks.

17.5 ± 1.3 kg C m^{-2} thawed over the course of 9 years and 24.0 ± 1.4 kg C m^{-2} thawed using thaw penetration. This meant that in control plots, using thaw penetration to calculate the quantity of newly thawed C resulted in an increase of 37 ± 10% relative to estimates calculated with ALT. In warming plots, we found an average of 41.0 ± 0.8 kg C m^{-2} in the active layer in 2009. By 2018, there was 67.8 ± 1.3 kg C m^{-2} in the active layer as calculated with ALT and 98.1 ± 1.7 kg C m^{-2} as calculated with thaw penetration. Therefore, over the course of 9 years, we calculated 26.8 ± 1.5 kg C m^{-2} thawed using ALT and 57.1 ± 1.2 kg C m^{-2} thawed using thaw penetration. This meant that in warming plots, using thaw penetration to calculate the quantity of newly thawed C resulted in an increase of 113 ± 6% relative to estimates calculated with ALT. Although ignoring subsidence does not impact direct measurements of soil C content, using ALT rather than thaw penetration to calculate C exposure in the active layer underestimates the rate of C exposure.
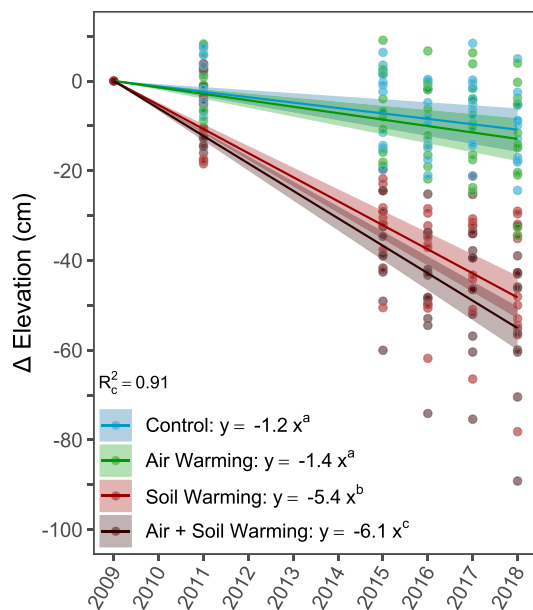
4.3. Drivers of Subsidence

Ice loss was the main environmental driver of subsidence at the site, but soil loss was a significant driver of subsidence, as well. Excess ice height did not correlate with subsidence, but total ice height did (Tables S2 and S3). The magnitude of subsidence was 95% (CI: 52, 138) of total ice height, and this relationship did not differ between control and soil warming treatments (Figure 6 and Table S3). Given that total ice height is necessarily an overestimate of the contribution of ice to subsidence, as some of the total ice volume must occupy pore space and not contribute to subsidence, the contribution of soil loss to subsidence was used to adjust the estimate of the contribution of ice loss to subsidence. Using eddy covariance data on C loss, we estimated that 9% of the measured subsidence could be due to soil loss, and using soil cores, we estimated 15%. If 9–15% of subsidence was due to soil loss, 85–91% of the measured subsidence remained to be explained by ice loss, and this corresponded to the loss of ~80–85% of the total ice volume from the thawed permafrost soil layer.

Figure 4. A mixed-effects model of subsidence (Δ elevation) by time and treatment. All intercepts were forced to zero, as the subsidence is necessarily zero during the first year. Control plots are shown in blue, air warming in green, soil warming in red, and air + soil warming in brown. Each point is a measurement from a single plot. The slope of each treatment is shown in the legend, and bands around the regression lines indicate 95% confidence intervals. Superscript letters indicate significant differences in slope. The interaction of time by treatment had a significant impact on subsidence. The slopes of the control and air warming treatments did not differ from each other, but the slopes of the soil warming and the air + soil warming treatments were different from each other and the other treatments.
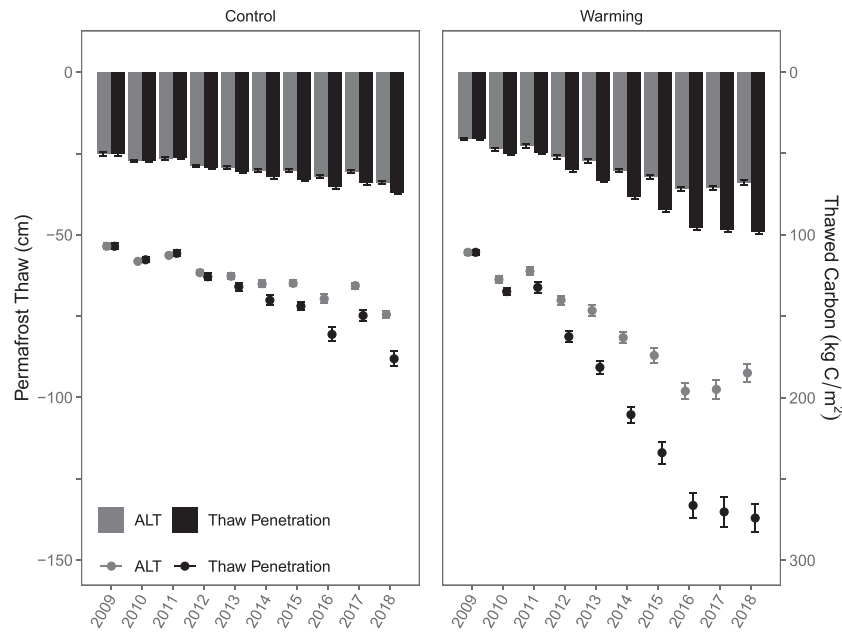
Figure 5. The impact of subsidence on observed permafrost thaw and C thaw. The points show permafrost thaw, as measured by ALT and thaw penetration, through time in control and soil warming plots. The bars show the amount of bulk soil C in the active layer, as measured from soil cores, and extrapolated to the field using ALT and thaw penetration. Error bars show SE.

4.4. Hydrologic Response to Subsidence

Subsidence at CiPEHR universally resulted in wetter soils, as subsidence caused the ground surface to drop closer to the water table, and this has consequences for energy transfer and C fluxes. In the most extreme cases in some of the soil warming plots, subsidence resulted in the formation of thermokarst ponds by 2016 and, despite 2017 and 2018 summer seasons having average to below average precipitation (Celis et al., 2018), the ponds rarely dried out in some plots. Even in areas that were not inundated, the water table depth moved closer to the soil surface over 9 years of warming, as the ground surface dropped closer to the water table in all treatments (Figure 7). The average water table depth in control plots in 2009 was 27.6 ± 0.4 cm, and in 2018, it was 18.4 ± 0.3 cm, 33% closer to the soil surface. In the soil warming plots, the average water table depth in 2009 was 25.4 ± 0.5 cm, and in 2018, it was 6.6 ± 0.3 cm, 74% closer to the soil surface. The increasingly wet conditions are increasing CH_4 fluxes due to anoxic conditions (Taylor et al., 2018) and are likely speeding the rate of thaw through increased energy transfer in water (Jorgenson et al., 2006; Jorgenson et al., 2010; Subin et al., 2013).
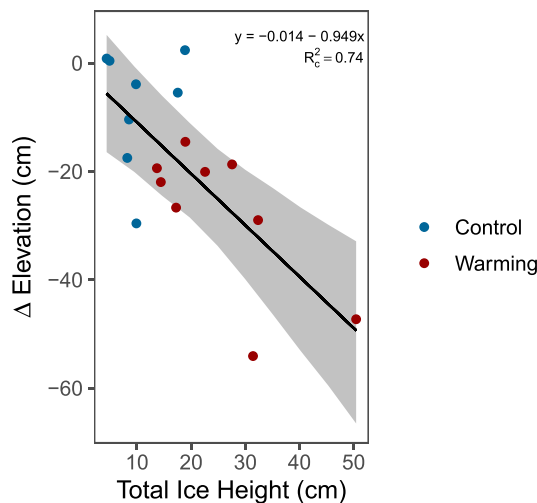

Figure 6. A mixed-effects model of subsidence by total ice height (sum of 2009 ice volume between the 2009 and final thaw penetration/soil core area). The band around the regression line indicates the 95% confidence interval. Subsidence was $95 \pm 43\%$ the magnitude of total ice height, and experimental treatment did not have an effect on the relationship.

5. Discussion

5.1. Subsidence Masks Total Permafrost Thaw

Subsidence was ubiquitous across treatments at CiPEHR, and slight increases in temperature were sufficient to dramatically accelerate this process. Both control and experimental warming plots are subsiding at CiPEHR, with gradual subsidence occurring in control plots and more rapid subsidence leading to thermokarst formation in soil warming plots. Gradual subsidence in the control plots left no visible features, despite an average of over 10 cm of subsidence over 9 years. Rates of subsidence in soil warming plots were over 4× higher than in control plots and ~5× higher in air + soil warming plots, leading to
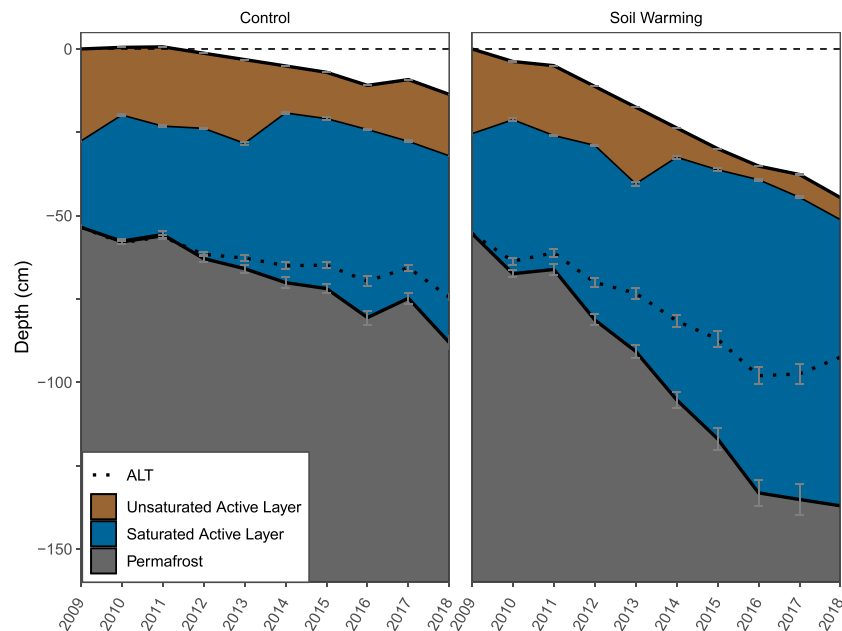
Figure 7. The average soil profile in control and soil warming plots. The active layer is between the soil surface and the thaw penetration, both shown as bold lines, and is broken into the layer above the water table and the layer below the water table. The unsaturated active layer (above the water table) is shown in brown, and the saturated active layer (below the water table) is shown in blue. Permafrost is shown in gray. The original soil surface is indicated with the dashed line, and the soil surface (upper bold line) has dropped from the original soil surface due to subsidence. The dotted line shows the ALT, and the lower bold line shows the thaw penetration. The ALT is shallower than thaw penetration within the soil profile, because using ALT relies on the assumption that the soil surface has not shifted from the original soil surface. The thaw penetration reflects the full depth of permafrost thaw, because it accounts for the change in height of the soil surface. Gray error bars indicate standard error of subsidence, water table depth, ALT, and thaw penetration measurements.

visible thermokarst formation in the most extreme cases. Thermokarst depressions became inundated starting around 2016 and were similar to other thermokarst features that have been identified in the area without experimental warming (Osterkamp et al., 2009). Based on previous research showing that open top chambers mostly affect air temperatures and not soil temperatures (Hobbie & Chapin, 1998; Marion et al., 1997; Shaver et al., 2000), we had not expected air warming to affect subsidence. Despite this, air + soil warming plots subsided more quickly than soil warming plots, although air warming alone had no impact on the rate of subsidence. This could be due to slightly higher deep soil temperatures during the summer season in air + soil warming plots relative to soil warming plots (Mauritz et al., 2017). It is also possible that open top chambers in inundated air + soil warming plots could reduce surface water flow sufficiently to increase water temperature and thereby increase thaw and subsidence at those locations, although we have no measurements of water temperature to confirm this.

ALT measurements at CiPEHR underestimate the thaw of permafrost, and the C it contains, due to the large magnitude of subsidence across all treatments. After 9 years, thaw penetration was 49% greater than ALT in soil warming plots and 19% greater than ALT in control plots. This is similar to the findings of two studies that did not experimentally warm soils, with thaw penetration being ~20% to >50% greater than ALT (O'Neill et al., 2019; Streletskiy et al., 2017). Additionally, we showed that this increased rate of permafrost thaw corresponded to a doubling of the rate of C thaw. This highlights the importance of complementing ALT measurements with subsidence measurements not just for understanding permafrost thaw but also for understanding the permafrost C feedback to the climate. The CALM network has made historical ALT measurements in many sites across the circumpolar region. Some of the CALM sites, such as the sites set up in the Mackenzie Valley by the Geological Survey of Canada, use thaw tubes that concurrently track elevation changes (Nixon & Taylor, 1998), but not all sites are accompanied by subsidence measurements. Without concurrent subsidence measurements, it is impossible to determine whether trends in ALT reflect trends in permafrost thaw, especially in the case of gradual, visually undetectable subsidence. Given that thermokarst features are estimated to cover ~20% of the permafrost zone (Olefeldt et al., 2016) and the potential for gradual subsidence to exist without any indication, it is necessary for quantification of subsidence to

occur at a broader scale and be accounted for when quantifying permafrost thaw. With the expanding availability of LiDAR to determine subsidence rates across entire landscapes, this problem is becoming more tractable, but it is still necessary to track elevation for validation at sites distributed across the circumpolar region.

5.2. Ice Loss and Soil Loss Drive Subsidence

Over 9 years of experimental warming at this site, ice loss was the main contributor to subsidence, accounting for 85–91% of the total subsidence. In permafrost soils, ice exists both within pore spaces and as excess ice that cannot fit within pore spaces, and it is excess ice that is expected to contribute to subsidence (Kokelj & Burn, 2003). However, when we estimated excess ice content using a published value of pore space, excess ice height was far too low to account for subsidence and did not correlate with subsidence (Figure S4 and Table S2). This indicates that the published value of pore space we used in our calculations may have been higher than the actual pore space in soils at CiPEHR. Therefore, our estimate of the contribution of ice loss to subsidence was calculated using the total ice volume to get an overestimate and then adjusted downward using the estimate of the contribution of organic matter loss to subsidence. Ice loss due to permafrost thaw is recognized as the main contributor to subsidence, including thermokarst formation, where erosion is limited (Jorgenson & Osterkamp, 2005; Kokelj & Jorgenson, 2013; Osterkamp et al., 2009). Since the landscape is relatively flat at this site (~5% slope), we do not observe erosion to be a significant contributor to subsidence as it is in coastal permafrost and retrogressive thaw slumps, for example. The spatial variability of subsidence at this site is likely due to the uneven distribution of ice (observed values of total permafrost ice content prior to thaw in soil cores range from 248–778 g kg^{-1}), and the locations with the highest ice content in the newly thawed active layer tended to experience the most subsidence, as has been observed in previous studies (Jorgenson & Osterkamp, 2005). This heterogeneity of both ice content and subsidence indicates that although subsidence in the control plots was not noticeable without measurements, it cannot be classified as isotropic subsidence and will likely result in thermokarst pits with continued thaw.

We estimated that 9–15% of the total subsidence was due to soil loss, with the lower bound being estimated from C fluxes to the atmosphere only and the upper bound being estimated from both C fluxes to the atmosphere and laterally in water. In reality, the soil loss is likely due to both C fluxes to the atmosphere and lateral transport of C in water (Cory et al., 2013; Lee et al., 2010; Plaza et al., 2019; Vogel et al., 2009), but additional direct measurements of lateral rates of C loss at the site are needed to strengthen our confidence in the magnitude of this effect on subsidence. Although this type of partitioning has not previously been published for permafrost ecosystems, we did find one study from a drained ombrotrophic bog in Norway, where 38% of subsidence over a 25 year period following drainage was due to peat loss (Grønlund et al., 2008), indicating that the decomposition of C-rich soils can contribute quite significantly to subsidence. Additionally, the contribution of soil loss to subsidence at this site is supported by several studies in tundra ecosystems that have found lower C content in soils within thermokarst features (Mu et al., 2016; Pizano et al., 2014).

The soil loss we observed can be explained by both the lateral loss of C in the form of dissolved and particulate organic C (Cory et al., 2013; Plaza et al., 2019) and CO_2 and CH_4 fluxes to the atmosphere (Lee et al., 2010; Vogel et al., 2009). Lateral loss of C has been both directly observed at the site, with greater summer season dissolved organic C concentrations in soil warming plots than control plots (Romano, 2018), and also inferred due to greater C loss from soil cores than can be explained by CO_2 and CH_4 fluxes (Plaza et al., 2019). Loss of C to the atmosphere is supported by measurements of CO_2 fluxes both in the area at large (Celis et al., 2017) and at CiPEHR specifically, which show more C loss from warming plots where subsidence is higher (Mauritz et al., 2017). Methane fluxes also correspond to deeper ALT and wetter microsites, and these environmental conditions were observed in soil warming plots that have subsided the most (Taylor et al., 2018).

5.3. Circumpolar Implications

Due to the widespread nature of subsidence in the permafrost zone, ignoring subsidence in measurements of permafrost thaw could be resulting in underestimates of thawed C stocks across the circumpolar region. The size of this underestimate depends mostly upon ice content in permafrost, which is often quite high. For example, on the Beaufort coast of Alaska, ice content varies from 43% in sandy areas to 89% in yedoma (Kanevskiy et al., 2013). Because large portions of the permafrost zone contain high ice volume and loss

of ice upon thaw drives the majority of subsidence, it follows that the soil surface height, which serves as a reference for ALT measurements, is shifting across the region. Therefore, it is necessary to quantify subsidence and incorporate it into measures of permafrost thaw, as is done with thaw penetration. Using thaw penetration as the measure of permafrost thaw across the permafrost region will also improve estimates of the thawed C pool (Nixon & Taylor, 1998). This is especially important because it is estimated that thermokarst features cover ~20% of the permafrost zone and contain ~50% of the C stored in permafrost (Olefeldt et al., 2016) and areas of thermokarst are likely to be the places with the largest discrepancy between ALT and thaw penetration. Of course, while the discrepancy between ALT and thaw penetration is not as great in areas of gradual subsidence, the potential for subsidence to occur without visual indication and the paucity of subsidence measurements means that it could be occurring at broad scales without human knowledge. Additionally, as more C is thawed in permafrost soils and exposed to increasingly wet conditions caused by subsidence, the release of C as both CO_2 and CH_4 could increase, thereby amplifying the warming potential of C fluxes from permafrost ecosystems (Burke et al., 2019; Cassidy et al., 2016; Turetsky et al., 2020; Walter Anthony et al., 2016).

The impact of subsidence on observed permafrost thaw at this relatively southern site serves as a clue of what the future may hold for more northerly sites. Our control plots represent current conditions at the southern extent of permafrost in the discontinuous permafrost zone, and despite the prevalence of abrupt thaw at higher latitudes (Olefeldt et al., 2016; Turetsky et al., 2020), gradual thaw and the resulting subsidence are likely occurring more quickly in the discontinuous permafrost zone than sites at higher latitudes. However, even in more northerly areas with relatively cold permafrost and shallow active layers, subsidence is already having a noticeable impact on observed permafrost thaw. Previously quantified rates of subsidence on the North Slope of Alaska have ranged from a low of 1–4 cm per decade (Liu et al., 2010) to >2.0 cm year^{-1} over 5 years (Streletskiy et al., 2008), and in the western Canadian Arctic, subsidence of 0.4 cm year^{-1} has been observed over 25 years (O'Neill et al., 2019). These rates are likely to increase in the near future, resulting in faster C release and irreversible changes to permafrost structure and ecosystem function (Schuur & Mack, 2018; Turetsky et al., 2020). Ecosystem function is likely to shift as hydrologic conditions change following subsidence, making it necessary to incorporate subsidence into estimates of C fluxes in Earth System Models (Ekici et al., 2019). Incorporation of subsidence into Earth System Models must also be accompanied by increased field monitoring to assess model performance and should occur both through the expansion of the network of thaw tubes and remote sensing of subsidence, for example, through LiDAR.

6. Conclusions

We observed subsidence rates of 1.2–6.1 cm year^{-1} at a permafrost warming experiment near the southern extent of permafrost, with the lowest rates occurring in control plots and the highest rates occurring in air + soil warming plots. A 5× increase in subsidence was instigated with warming of only 1–2°C in both air and soil temperatures, as permafrost temperatures are already near 0°C. The subsidence was explained by the combined impact of ice and soil loss, with ice loss driving the majority of subsidence. Additionally, subsidence is causing a shifting reference frame for ALT measurements, the traditional measure of permafrost thaw. Ignoring the impact of subsidence on permafrost thaw underestimates total permafrost thaw over timescales as short as a few years to a decade. We found that using thaw penetration to measure the permafrost thaw in control and permafrost warming plots increased observed permafrost thaw by 19–49% and the observed amount of newly thawed C by 37–113%. Because of the potential for subsidence to impact much of the permafrost zone and the C it contains, it is imperative that studies of permafrost thaw incorporate measurements of subsidence in order to understand the full impact of climate change on permafrost stability and C release from permafrost ecosystems. Future efforts to quantify subsidence should focus on using LiDAR data, which allow the quick quantification of subsidence over broad scales.

References

Abbott, B. W., & Jones, J. B. (2015). Permafrost collapse alters soil carbon stocks, respiration, CH_4, and N_2O in upland tundra. *Global Change Biology*, *21*(12), 4570–4587. https://doi.org/10.1111/gcb.13069

Abbott, B. W., Jones, J. B., Godsey, S. E., Larouche, J. R., & Bowden, W. B. (2015). Patterns and persistence of hydrologic carbon and nutrient export from collapsing upland permafrost. *Biogeosciences*, *12*(12), 3725–3740. https://doi.org/10.5194/bg-12-3725-2015

Bates, D., Maechler, M., Bolker, B., & Walker, S. (2015). Fitting linear mixed-effects models using lme4. *Journal of Statistical Software*, *67*(1), 1–48. https://doi.org/10.18637/jss.v067.i01

Belshe, E. F., Schuur, E. A. G., & Bolker, B. M. (2013). Tundra ecosystems observed to be CO_2 sources due to differential amplification of the carbon cycle. *Ecology Letters*, *16*(10), 1307–1315. https://doi.org/10.1111/ele.12164

Belshe, E. F., Schuur, E. A. G., Bolker, B. M., & Bracho, R. (2012). Incorporating spatial heterogeneity created by permafrost thaw into a landscape carbon estimate. *Journal of Geophysical Research*, *117*, G01026. https://doi.org/10.1029/2011JG001836

Bivand, R. S., Pebesma, E. J., & Gómez-Rubio, V. (2008). In R. Gentleman, K. Hornik, & G. Parmigiani (Eds.), *Applied spatial data analysis with R*. New York, NY: Springer Science+Business Media, LLC.

Blanc-Betes, E., Welker, J. M., Sturchio, N. C., Chanton, J. P., & Gonzalez-Meler, M. A. (2016). Winter precipitation and snow accumulation drive the methane sink or source strength of Arctic tussock tundra. *Global Change Biology*, *22*(8), 2818–2833. https://doi.org/10.1111/gcb.13242

Brady, N. C., & Weil, R. R. (2008). *The nature and properties of soils* (14th ed.). Upperson Saddle River, NJ: Pearson Education, Inc.

Brown, J., Hinkel, K. M., & Nelson, F. E. (2000). The Circumpolar Active Layer Monitoring (CALM) program: Research designs and initial results. *Polar Geography*, *24*(3), 165–258. https://doi.org/10.1080/10889370009377698

Burke, S. A., Wik, M., Lang, A., Contosta, A. R., Palace, M., Crill, P. M., & Varner, R. K. (2019). Long-term measurements of methane ebullition from thaw ponds. *Journal of Geophysical Research: Biogeosciences*, *124*, 2208–2221. https://doi.org/10.1029/2018JG004786

Cassidy, A. E., Christen, A., & Henry, G. H. R. (2016). The effect of a permafrost disturbance on growing-season carbon-dioxide fluxes in a high Arctic tundra ecosystem. *Biogeosciences*, *13*(8), 2291–2303. https://doi.org/10.5194/bg-13-2291-2016

Celis, G., Mauritz, M., Bracho, R., Salmon, V. G., Webb, E. E., Hutchings, J., et al. (2017). Tundra is a consistent source of CO_2 at a site with progressive permafrost thaw during 6 years of chamber and eddy covariance measurements. *Journal of Geophysical Research: Biogeosciences*, *122*, 1471–1485. https://doi.org/10.1002/2016JG003671

Celis, G., Mauritz, M., Taylor, M. A., Ledman, J. D., Natali, S. M., & Schuur, E. A. G. (2018). *Eight Mile Lake Research Watershed: Hourly meteorological data, 2004–2018*. Bonanza Creek LTER—University of Alaska Fairbanks. BNZ:453. https://doi.org/10.6073/pasta/ec2da48c393574c7b62baa8140c86ae8

Chapin, F. S., Shaver, G. R., Giblin, A. E., Nadelhoffer, K. J., & Laundre, J. A. (1995). Responses of Arctic tundra to experimental and observed changes in climate. *Ecology*, *76*(3), 694–711. https://doi.org/10.2307/1939337

Commane R, Lindaas J, Benmergui J, Luus K. A., Chang R. Y.-W., Daube B. C., Euskirchen E. S., Henderson J. M., Karion A, Miller J. B., Miller S. M., Parazoo N. C., Randerson J. T., Sweeney C, Tans P, Thoning K, Veraverbeke S, Miller C. E., Wofsy S. C. (2017). Carbon dioxide sources from Alaska driven by increasing early winter respiration from Arctic tundra. *Proceedings of the National Academy of Sciences*, *114*, (21), 5361–5366. https://doi.org/10.1073/pnas.1618567114

Cory, R. M., Crump, B. C., Dobkowski, J. A., & Kling, G. W. (2013). Surface exposure to sunlight stimulates CO_2 release from permafrost soil carbon in the Arctic. *Proceedings of the National Academy of Sciences*, *110*(9), 3429–3434. https://doi.org/10.1073/pnas.1214104110

Ekici, A., Lee, H., Lawrence, D. M., Swenson, S. C., & Prigent, C. (2019). Ground subsidence effects on simulating dynamic high-latitude surface inundation under permafrost thaw using CLM5. *Geoscientific Model Development*, *12*(12), 5291–5300. https://doi.org/10.5194/gmd-12-5291-2019

Euskirchen, E. S., Edgar, C. W., Syndonia Bret-Harte, M., Kade, A., Zimov, N., & Zimov, S. (2017). Interannual and seasonal patterns of carbon dioxide, water, and energy fluxes from ecotonal and thermokarst-impacted ecosystems on carbon-rich permafrost soils in northeastern Siberia. *Journal of Geophysical Research: Biogeosciences*, *122*, 2651–2668. https://doi.org/10.1002/2017JG004070

Gräler, B., Pebesma, E. J., & Heuvelink, G. (2016). Spatio-temporal interpolation using gstat. *The R Journal*, *8*(1), 204–218. https://doi.org/10.32614/rj-2016-014

Grønlund, A., Hauge, A., Hovde, A., & Rasse, D. P. (2008). Carbon loss estimates from cultivated peat soils in Norway: A comparison of three methods. *Nutrient Cycling in Agroecosystems*, *81*(2), 157–167. https://doi.org/10.1007/s10705-008-9171-5

Hicks Pries, C. E., Schuur, E. A. G., & Crummer, K. G. (2012). Holocene carbon stocks and carbon accumulation rates altered in soils undergoing permafrost thaw. *Ecosystems*, *15*(1), 162–173. https://doi.org/10.1007/s10021-011-9500-4

Hicks Pries, C. E., Schuur, E. A. G., & Crummer, K. G. (2013). Thawing permafrost increases old soil and autotrophic respiration in tundra: Partitioning ecosystem respiration using ^{13}C and ^{14}C. *Global Change Biology*, *19*(2), 649–661. https://doi.org/10.1111/gcb.12058

Hicks Pries, C. E., Schuur, E. A. G., Natali, S. M., & Crummer, K. G. (2016). Old soil carbon losses increase with ecosystem respiration in experimentally thawed tundra. *Nature Climate Change*, *6*(2), 214–218. https://doi.org/10.1038/nclimate2830

Hijmans, R. (2019). *raster: Geographic data analysis and modeling (version R package version 2.8–19)*. Retrieved from https://CRAN.R-project.org/package=raster

Hinkel, K. M., & Hurd, J. K. (2006). Permafrost destabilization and thermokarst following snow fence installation, Barrow, Alaska, USA. *Arctic, Antarctic, and Alpine Research*, *38*(4), 530–539. https://doi.org/10.1657/1523-0430(2006)38[530:PDATFS]2.0.CO;2

Hinkel, K. M., & Nelson, F. E. (2003). Spatial and temporal patterns of active layer thickness at Circumpolar Active Layer Monitoring (CALM) sites in northern Alaska, 1995–2000. *Journal of Geophysical Research*, *108*(D2), 8168. https://doi.org/10.1029/2001JD000927

Hobbie, S. E., & Chapin, F. S. (1998). The response of tundra plant biomass, aboveground production, nitrogen, and CO_2 flux to experimental warming. *Ecology*, *79*(5), 1526–1544. https://doi.org/10.1890/0012-9658(1998)079[1526:TROTPB]2.0.CO;2

Houghton, R. A. (2007). Balancing the global carbon budget. *Annual Review of Earth and Planetary Sciences*, *35*(1), 313–347. https://doi.org/10.1146/annurev.earth.35.031306.140057

Intergovernmental Panel on Climate Change (2013). *Climate change 2013: The physical science basis. Contribution of Working Group I to the Fifth Assessment Report of the Intergovernmental Panel on Climate Change*. Cambridge, United Kingdom and New York, NY, USA: Cambridge University Press.

Johansson, M., Callaghan, T. V., Bosiö, J., Åkerman, H. J., Jackowicz-Korczynski, M., & Christensen, T. R. (2013). Rapid responses of permafrost and vegetation to experimentally increased snow cover in sub-arctic Sweden. *Environmental Research Letters*, *8*(3), 035025. https://doi.org/10.1088/1748-9326/8/3/035025

Johnston, C. E., Ewing, S. A., Harden, J. W., Varner, R. K., Wickland, K. P., Koch, J. C., et al. (2014). Effect of permafrost thaw on CO_2 and CH_4 exchange in a western Alaska peatland chronosequence. *Environmental Research Letters*, *9*(8), 085004. https://doi.org/10.1088/1748-9326/9/8/085004

Jones, M. C., Grosse, G., Jones, B. M., & Walter Anthony, K. (2012). Peat accumulation in drained thermokarst lake basins in continuous, ice-rich permafrost, northern Seward Peninsula, Alaska. *Journal of Geophysical Research*, *117*, G00M07. https://doi.org/10.1029/2011JG001766

Jorgenson, M. T., Harden, J., Kanevskiy, M., O'Donnell, J., Wickland, K., Ewing, S., et al. (2013). Reorganization of vegetation, hydrology and soil carbon after permafrost degradation across heterogeneous boreal landscapes. *Environmental Research Letters*, *8*(3), 035017. https://doi.org/10.1088/1748-9326/8/3/035017

Jorgenson, M. T., & Osterkamp, T. E. (2005). Response of boreal ecosystems to varying modes of permafrost degradation. *Canadian Journal of Forest Resources*, *35*(9), 2100–2111. https://doi.org/10.1139/X05-153

Jorgenson, M. T., Romanovsky, V., Harden, J., Schur, Y., O'Donnell, J. A., Schuur, E. A. G., et al. (2010). Resilience and vulnerability of permafrost to climate change. *Canadian Journal of Forest Research*, *40*(7), 1302–1312. https://doi.org/10.1139/X10-061

Jorgenson, M. T., Shur, Y. L., & Pullman, E. R. (2006). Abrupt increase in permafrost degradation in Arctic Alaska. *Geophysical Research Letters*, *33*, L02503. https://doi.org/10.1029/2005GL024960

Kanevskiy, M. Z., Shur, Y. L., Jorgenson, M. T., Ping, C.-L., Michaelson, G. J., Fortier, D., et al. (2013). Ground ice in the upper permafrost of the Beaufort Sea coast of Alaska. *Cold Regions Science and Technology*, *85*, 56–70. https://doi.org/10.1016/j.coldregions.2012.08.002

Kokelj S. V., & Burn C. R. (2003). Ground ice and soluble cations in near-surface permafrost, Inuvik, Northwest Territories, Canada. *Permafrost and Periglacial Processes*, *14*, (3), 275–289. https://doi.org/10.1002/ppp.458

Kokelj, S. V., & Jorgenson, M. T. (2013). Advances in thermokarst research: Recent advances in research investigating thermokarst processes. *Permafrost and Periglacial Processes*, *24*(2), 108–119. https://doi.org/10.1002/ppp.1779

Kutzbach, L., Wagner, D., & Pfeiffer, E. M. (2004). Effect of microrelief and vegetation on methane emission from wet polygonal tundra, Lena Delta, northern Siberia. *Biogeochemistry*, *69*(3), 341–362. https://doi.org/10.1023/B:BIOG.0000031053.81520.db

Lee, H., Schuur, E. A. G., & Vogel, J. G. (2010). Soil CO_2 production in upland tundra where permafrost is thawing. *Journal of Geophysical Research*, *115*, G01009. https://doi.org/10.1029/2008JG000906

Lenth, R. (2018). *Emmeans: Estimated marginal means, aka least-squares means (version R package version 1.2.4.)*. Retrieved from https://CRAN.R-project.org/package=emmeans

Liu, L., Zhang, T., & Wahr, J. (2010). InSAR measurements of surface deformation over permafrost on the north slope of Alaska. *Journal of Geophysical Research*, *115*, 1–14. https://doi.org/10.1029/2009JF001547

Marion, G. M., Henry, G. H. R., Freckman, D. W., Johnstone, J., Jones, G., Jones, M. H., et al. (1997). Open-top designs for manipulating field temperature in high-latitude ecosystems. *Global Change Biology*, *3*(S1), 20–32. https://doi.org/10.1111/j.1365-2486.1997.gcb136.x

Mauritz, M., Bracho, R., Celis, G., Hutchings, J., Natali, S. M., Pegoraro, E. F., et al. (2017). Nonlinear CO_2 flux response to 7 years of experimentally induced permafrost thaw. *Global Change Biology*, *23*(9), 3646–3666. https://doi.org/10.1111/gcb.13661

Mu, C., Zhang, T., Zhang, X., Li, L., Guo, H., Zhao, Q., et al. (2016). Carbon loss and chemical changes from permafrost collapse in the northern Tibetan plateau: Permafrost collapse caused carbon loss. *Journal of Geophysical Research: Biogeosciences*, *121*, 1781–1791. https://doi.org/10.1002/2015JG003235

Myhre, G, Shindell, D, Bréon, F., Collins, W., Fuglestvedt, J., Huang, J., et al. (2013). Anthropogenic and natural radiative forcing. In *Climate change* (pp. 659–740). Cambridge, United Kingdom: Cambridge University Press.

Natali, S. M., & Schuur, E. A. G. (2012). *Eight Mile Lake Research Watershed, Carbon in Permafrost Experimental Heating Research (CiPEHR): Seasonal water table depth data, 2009–2011*. Bonanza Creek LTER—University of Alaska Fairbanks. BNZ:497. https://doi.org/10.6073/pasta/3e21d3282f68c6d5c927f0a7221f9fc5

Natali, S. M., Schuur, E. A. G., Trucco, C., Hicks Pries, C. E., Crummer, K. G., & Baron Lopez, A. F. (2011). Effects of experimental warming of air, soil and permafrost on carbon balance in Alaskan tundra. *Global Change Biology*, *17*(3), 1394–1407. https://doi.org/10.1111/j.1365-2486.2010.02303.x

National Ecological Observatory Network (2017a). *Data product DP3.30024.001, elevation—LiDAR*. Batelle. data.neonscience.org

National Ecological Observatory Network. (2017b). *Data product DP1.10047.001, soil physical properties (distributed initial characterization)*. http://data.neonscience.org

National Ecological Observatory Network (2018). *Data product DP1.30010.001, high-resolution orthorectified camera imagery*. Batelle. http://data.neonscience.org

Nelson, F. E., Anisimov, O. A., & Shiklomanov, N. I. (2001). Subsidence risk from thawing permafrost. *Nature*, *410*(6831), 889–890. https://doi.org/10.1038/35073746

Nixon, F. M., & Taylor, A. E. (1998). Regional active layer monitoring across the sporadic, discontinuous and continuous permafrost zones, Mackenzie Valley, northwestern Canada. In *Proceedings of the 7th International Permafrost Conference* (Vol. 55, pp. 815–820). Quebec City, QC: Collection Nordicana.

O'Neill, H. B., & Burn, C. R. (2017). Talik formation at a snow fence in continuous permafrost, Western Arctic Canada. *Permafrost and Periglacial Processes*, *28*(3), 558–565. https://doi.org/10.1002/ppp.1905

O'Neill, H. B., Smith, S. L., & Duchesne, C. (2019). Long-term permafrost degradation and thermokarst subsidence in the Mackenzie Delta area indicated by thaw tube measurements. *Cold Regions Engineering*, *2019*, 643–651. https://doi.org/10.1061/9780784482599.074

Olefeldt, D., Goswami, S., Grosse, G., Hayes, D. J., Hugelius, G., Kuhry, P., et al. (2016). Circumpolar distribution and carbon storage of thermokarst landscapes. *Nature Communications*, *7*(1), 1–11. https://doi.org/10.1038/ncomms13043

Osterkamp, T. E., Jorgenson, M. T., Schuur, E. A. G., Shur, Y. L., Kanevskiy, M. Z., Vogel, J. G., & Tumskoy, V. E. (2009). Physical and ecological changes associated with warming permafrost and thermokarst in interior Alaska. *Permafrost and Periglacial Processes*, *20*(3), 235–256. https://doi.org/10.1002/ppp.656

Pebesma, E. J. (2004). *Multivariable geostatistics in S: The gstat package*, (Vol. 30, pp. 683–691).

Pegoraro, E. F., Mauritz, M., Bracho, R., Ebert, C., Dijkstra, P., Hungate, B. A., et al. (2019). Glucose addition increases the magnitude and decreases the age of soil respired carbon in a long-term permafrost incubation study. *Soil Biology and Biochemistry*, *129*, 201–211. https://doi.org/10.1016/j.soilbio.2018.10.009

Pegoraro, E. F., Mauritz, M., Hutchings, J. A., Natali, S. M., & Schuur, E. A. G. (2019). *Eight Mile Lake Research Watershed, Carbon in Permafrost Experimental Heating Research (CiPEHR): Weekly thaw depth data, 2009–2018*. Bonanza Creek LTER—University of Alaska Fairbanks. BNZ:480. https://doi.org/10.6073/pasta/894ec9847bc365347775d3aaba44a502

Phillips, M. R., Burn, C. R., Wolfe, S. A., Morse, P. D., Gaanderse, A. J., O'Neill, H. B., Shugar, D. H., & Gruber, S. (2015). Improving water content description of ice-rich permafrost soils. *Proceedings GeoQuébec*, *68*,

Pizano, C., Barón, A. F., Schuur, E. A. G., Crummer, K. G., & Mack, M. C. (2014). Effects of thermo-erosional disturbance on surface soil carbon and nitrogen dynamics in upland arctic tundra. *Environmental Research Letters*, *9*(7), 075006. https://doi.org/10.1088/1748-9326/9/7/075006

Plaza, C., Pegoraro, E. F., Bracho, R., Celis, G., Crummer, K. G., Hutchings, J. A., et al. (2019). Direct observation of permafrost degradation and rapid soil carbon loss in tundra. *Nature Geoscience*, *12*(8), 627–631. https://doi.org/10.1038/s41561-019-0387-6

Plaza, C., Schuur, E. A. G., & Pegoraro, E. F. (2017). *Eight Mile Lake Research Watershed, Carbon in Permafrost Experimental Heating Research (CiPEHR): Physical and chemical properties of soils, 2009–2013*. Bonanza Creek LTER—University of Alaska Fairbanks. BNZ:655. https://doi.org/10.6073/pasta/f502d8fe1a2e1d6c6b035c198af04f3e

R Core Team (2018). *R: A language and environment for statistical computing*. Retrieved from https://www.R-project.org/

Rodenhizer, H., Mauritz, M., Taylor, M. A., Ledman, J. D., Natali, S. M., & Schuur, E. A. G. (2019a). *Eight Mile Lake Research Watershed, Carbon in Permafrost Experimental Heating Research (CiPEHR): GPS elevation, 2009–2019*. Bonanza Creek LTER—University of Alaska Fairbanks. BNZ:729. https://doi.org/10.6073/pasta/9b181a01b52f254a9cdbcba007c0a165

Rodenhizer, H., Mauritz, M., Taylor, M. A., Ledman, J. D., Natali, S. M., & Schuur, E. A. G. (2019b). *Eight Mile Lake Research Watershed, Carbon in Permafrost Experimental Heating Research (CiPEHR): GPS plot locations*. Bonanza Creek LTER—University of Alaska Fairbanks. BNZ:730. https://doi.org/10.6073/pasta/9b181a01b52f254a9cdbcba007c0a165

Romano, E. (2018). *Dissolved organic carbon released from thawing permafrost soils and detected in headwater streams*, Flagstaff, Arizona: Northern Arizona University. Retrieved from ProQuest Theses and Dissertations

Romanovsky, V. E., Sergueev, D. O., & Osterkamp, T. E. (2003). Temporal variations in the active layer and near-surface permafrost temperatures at the long-term observatories in northern Alaska. *Permafrost*, *1 and 2*, 989–994.

Salmon, V. G., Schädel, C., Bracho, R., Pegoraro, E. F., Celis, G., Mauritz, M., et al. (2018). Adding depth to our understanding of nitrogen dynamics in permafrost soils. *Journal of Geophysical Research: Biogeosciences*, *123*, 2497–2512. https://doi.org/10.1029/2018JG004518

Salmon, V. G., Soucy, P., Mauritz, M., Celis, G., Natali, S. M., Mack, M. C., & Schuur, E. A. G. (2016). Nitrogen availability increases in a tundra ecosystem during five years of experimental permafrost thaw. *Global Change Biology*, *22*(5), 1927–1941. https://doi.org/10.1111/gcb.13204

Schädel, C., Koven, C. D., Lawrence, D. M., Celis, G., Garnello, A. J., Hutchings, J., et al. (2018). Divergent patterns of experimental and model-derived permafrost ecosystem carbon dynamics in response to Arctic warming. *Environmental Research Letters*, *13*(10), 105,002. https://doi.org/10.1088/1748-9326/aae0ff

Schädel, C., Mauritz, M., Taylor, M. A., Ledman, J. D., Natali, S. M., & Schuur, E. A. G. (2018). *Eight Mile Lake Research Watershed, Carbon in Permafrost Experimental Heating Research (CiPEHR): Seasonal water table depth data, 2012–2018*. Bonanza Creek LTER—University of Alaska Fairbanks. BNZ:554. https://doi.org/10.6073/pasta/f5db5af592a52f546220efe0a496d36b

Schuur, E. A. G., Bockheim, J., Canadell, J. G., Euskirchen, E., Field, C. B., Goryachkin, S. V., et al. (2008). Vulnerability of permafrost carbon to climate change: Implications for the global carbon cycle. *Bioscience*, *58*(8), 701–714. https://doi.org/10.1641/B580807

Schuur, E. A. G., Crummer, K. G., Vogel, J. G., & Mack, M. C. (2007). Plant species composition and productivity following permafrost thaw and thermokarst in Alaskan tundra. *Ecosystems*, *10*(2), 280–292. https://doi.org/10.1007/s10021-007-9024-0

Schuur, E. A. G., & Mack, M. C. (2018). Ecological response to permafrost thaw and consequences for local and global ecosystem services. *Annual Review of Ecology, Evolution, and Systematics*, *23*, 279–301. https://doi.org/10.1146/annurev-ecolsys-121415-032349

Schuur, E. A. G., McGuire, A. D., Grosse, G., Harden, J. W., Hayes, D. J., Hugelius, G., et al. (2015). Climate change and the permafrost carbon feedback. *Nature*, *520*(7546), 171–179. https://doi.org/10.1038/nature14338

Schuur, E. A. G., McGuire, D. A., Romanovsky, V. E., Schädel, C., & Mack, M. C. (2018). Chapter 11: Arctic and boreal carbon. In N. Cavallaro, G. Shrestha, R. Birdsey, M. A. Mayes, R. G. Najjar, S. C. Reed, P. Romero-Lankao, & Z. Zhu (Eds.), *Second State of the Carbon Cycle Report (SOCCR2): A sustained assessment report* (pp. 428–468). Washington, DC: U.S. Global Change Research Program. https://doi.org/10.7930/SOCCR2.2018.Ch11

Shaver, G. R., Billings, W. D., Chapin, F. S., Giblin, A. E., Nadelhoffer, K. J., Oechel, W. C., & Rastetter, E. B. (1992). Global change and the carbon balance of Arctic ecosystems. *Bioscience*, *42*(6), 433–441. https://doi.org/10.2307/1311862

Shaver, G. R., Canadell, J., Chapin, F. S., Gurevitch, J., Harte, J., Henry, G., et al. (2000). Global warming and terrestrial ecosystems: A conceptual framework for analysis. *Bioscience*, *50*(10), 871. https://doi.org/10.1641/0006-3568(2000)050[0871:GWATEA]2.0.CO;2

Shiklomanov, N. I., Streletskiy, D. A., Little, J. D., & Nelson, F. E. (2013). Isotropic thaw subsidence in undisturbed permafrost landscapes. *Geophysical Research Letters*, *40*, 6356–6361. https://doi.org/10.1002/2013GL058295

Shiklomanov, N. I., Streletskiy, D. A., & Nelson, F. E. (2012). Northern Hemisphere component of the global Circumpolar Active Layer Monitoring (CALM) program. *Proceedings of the Tenth International Conference on Permafrost*, *1*, 377–382.

Streletskiy, D. A., Shiklomanov, N. I., Little, J. D., Nelson, F. E., Brown, J., Nyland, K. E., & Klene, A. E. (2017). Thaw subsidence in undisturbed tundra landscapes, Barrow, Alaska, 1962–2015. *Permafrost and Periglacial Processes*, *28*(3), 566–572. https://doi.org/10.1002/ppp.1918

Streletskiy, D. A., Shiklomanov, N. I., Nelson, F. E., & Klene, A. E. (2008). Thirteen years of observations at Alaskan CALM sites: Long-term active layer and ground surface temperature trends. *Proceedings of the 9th International Conference on Permafrost*, *2*, 1727–1732.

Subin, Z. M., Koven, C. D., Riley, W. J., Torn, M. S., Lawrence, D. M., & Swenson, S. C. (2013). Effects of soil moisture on the responses of soil temperatures to climate change in cold regions. *Journal of Climate*, *26*(10), 3139–3158. https://doi.org/10.1175/JCLI-D-12-00305.1

Tarnocai, C., Canadell, J. G., Schuur, E. A. G., Kuhry, P., Mazhitova, G., & Zimov, S. (2009). Soil organic carbon pools in the northern circumpolar permafrost region. *Global Biogeochemical Cycles*, *23*(2), 1–11. https://doi.org/10.1029/2008GB003327

Taylor, M. A., Celis, G., Ledman, J. D., Bracho, R., & Schuur, E. A. G. (2018). Methane efflux measured by eddy covariance in Alaskan upland tundra undergoing permafrost degradation. *Journal of Geophysical Research: Biogeosciences*, *123*, 2695–2710. https://doi.org/10.1029/2018JG004444

Turetsky, M. R., Abbott, B. W., Jones, M. C., Walter Anthony, K., Olefeldt, D., Schuur, E. A. G., et al. (2020). Carbon release through abrupt permafrost thaw. *Nature Geoscience*, *13*(2), 138–143. https://doi.org/10.1038/s41561-019-0526-0

Vogel, J., Schuur, E. A. G., Trucco, C., & Lee, H. (2009). Response of CO_2 exchange in a tussock tundra ecosystem to permafrost thaw and thermokarst development. *Journal of Geophysical Research*, *114*, G04018. https://doi.org/10.1029/2008JG000901

Walter Anthony, K. M., Daanen, R., Anthony, P., Schneider von Deimling, T., Ping, C.-L., Chanton, J. P., & Grosse, G. (2016). Methane emissions proportional to permafrost carbon thawed in Arctic lakes since the 1950s. *Nature Geoscience*, *9*(9), 679–682. https://doi.org/10.1038/ngeo2795

Ward Jones, M. K., Pollard, W. H., & Jones, B. M. (2019). Rapid initialization of retrogressive thaw slumps in the Canadian high Arctic and their response to climate and terrain factors. *Environmental Research Letters*, *14*(5), 055006. https://doi.org/10.1088/1748-9326/ab12fd

Wickham, H. (2017). *tidyverse: Easily install and load the "tidyverse" (version R package version 1.2.1)*. Retrieved from https://CRAN.R%2010project.org/package=tidyverse

Zimov, S. A., Davydov, S. P., Zimova, G. M., Davydova, A. I., Schuur, E. A. G., Dutta, K., & Chapin, F. S. (2006). Permafrost carbon: Stock and decomposability of a globally significant carbon pool. *Geophysical Research Letters*, *33*, L20502. https://doi.org/10.1029/2006GL027484